Conclusions

Information on soil development, erosion and deposition and the balance of these three processes indicates the extent of soil formation *vis-à-vis* soil loss in a landscape. Basic data on soils and the site characteristics are, therefore, important for determining degree of soil erosion to assess degradation of soils as well as the landscapes. Although all the sites described in our study are continuously eroded, the site 3 with soils containing huge clay is at a less degree of degradation than the soils at sites 1 and 2. While the soil degradation due to shifting cultivation and other human intervention can be controlled, the conservation of landscape degradation due to neotectonics is yet to be found out.

1. Oldeman, L. R. (ed.), Global assessment of soil degradation (GLASOD). Guidelines for general assessment of status of human-induced soil degradation, ISRIC, Wageningen, 1988.
2. Sehgal, J. and Arbrol, I. P., *Soil Degradation in India: Status and Impact*, Oxford & IBH Publishing Co. Pvt Ltd, New Delhi, 1994.
3. Mukhopadhyay, S. C., *Indian Geomorphology and Resource Management* (ed. Jog, S. R.), 3rd Annual Conference of Indian Institute of Geomorphologists, held at Pune in Nov. 1990.
4. Soil Survey Staff, *Soil Survey Manual, Agric. Handb. U.S. Dept. Agric.*, Washington DC, 1951.
5. Jackson, M. L., *Soil Chemical Analysis*, Prentice Hall of India Pvt Ltd, New Delhi, 1973.
6. Wischmeier, W. H., Johnson, C. B. and Cross, B. V., *J. Soil Water Conserv.*, 1971, **26**, 189–193.
7. Pal, D. K., Kalbande, A. R., Deshpande, S. B. and Sehgal, J. L., *Soil Sci.*, 1994, **158**, 465–473.
8. Barshad, I., in *Chemistry of the Soil* (ed. Bear, F. E.), Reinhold, New York, 1964, pp. 75–92.
9. Ellis, S., Taylor, D. M. and Masood, K. R., *Catena*, 1994, **22**, 69–78.
10. Singh, D. R. and Gupta, P. N., in Proceedings of the International Symposium on Hydrological Aspects of Mountainous Watersheds, University of Roorkee, Roorkee, 1982, pp. 60–66.
11. Narayana, D. V. V., *Mountain Res. Dev.*, 1987, **7**, 287–298.
12. Hadda, M. S. and Kukal, S. S., *Soil Use Management*, 1991, **7**, 45–47.
13. Singh, G., Babu Ram and Subhas Chandra, *Soil Loss Prediction Research in India*, ICAR Bulletin No. T-12/D-9, 1981.
14. Soil Survey Staff, *Keys to Soil Taxonomy*, 6th edn, 1994.

ACKNOWLEDGEMENTS. We thank Dr D. K. Pal, NBSS&LUP, Nagpur for his help during the preparation of this manuscript.

Received 26 August 1996; revised accepted 31 October 1997

Detection and identification of seismic signals using artificial neural networks

Falguni Roy

Seismology Section, High Pressure Physics Division, Bhabha Atomic Research Centre, Mumbai 400 085, India

Artificial neural networks (ANNs) are emerging as potential tools for the detection and identification of seismic signals owing to the fact that they can be adapted to fit more complex decision surfaces compared with the conventional techniques. This paper deals with the development of two ANNs, one for the purpose of on-line detection of seismic signals and the other for the identification of the signals. It has been demonstrated that these ANNs, trained with various parameters derived from the digital data as obtained from the Gauribidanur seismic array, India, have excellent capabilities to detect and identify weak seismic signals.

DETECTION and identification of seismic signals, having body wave magnitudes (mb) four or more, at teleseismic distances seem feasible with the presently available instruments and data analysis methods. However, identification of small magnitude events which could be recorded only at regional distances (< 2000 km) requires significant efforts to devise techniques for detecting, analysing and interpreting such regional data. With ever-increasing inflow rate of digital data, on-line processing of seismic data has become a necessity. Modern high speed digital computers have over the years made it possible for the users to implement various sophisticated processing algorithms to extract meaningful information from raw data. Presently, extensive research efforts are directed towards the designing of artificial neural networks (ANNs) which are conceived as promising solutions to various complex artificial intelligence problems like pattern and speech recognition[1–4]. ANNs are also emerging as potential tools in the field of seismic signal detection and identification.

The present paper deals with the development of two ANNs for the purpose of signal detection and identifi-

cation of the detected signals respectively. Short period (SP) digital data from Gauribidanur array, India (GBA) have been used for this study.

Artificial neural networks

The ANNs are designed to mimic the pattern recognition process of the human brain and are well suited to handle classification problems. In general, an ANN has an input layer, i.e. the layer of neurons through which the input data enters the network, one or more intermediate layers, also known as hidden layers, and an output layer which produces the output response of the network (Figure 1). In a fully connected ANN, neurons of each layer are connected to the neurons of the next layer through some weights W_{ji}, where i stands for the ith neuron of the previous layer and j stands for the jth neuron of the present layer. In a feed forward ANN, every neuron in lower unit must send its output to higher layers excluding its own neurons. Learning procedure begins with the presentation of an input vector to the input layer. The input, X_j, to the unit j is a linear function of the outputs, Y_i, of the neurons that are connected to j and the weights, W_{ji}, connecting these neurons

$$X_j = \sum_i Y_i W_{ji}. \tag{1}$$

Output of a neuron, Y_j, is obtained as a nonlinear function of its total input, X_j,

$$Y_j = 1/(1 + \exp(-X_j)). \tag{2}$$

These Y_j's, with values ranging between 0 and 1, form the input to the next layer. The learning procedure used, recursively adjusts the weights, W_{ji}, of the connections in the network by minimizing measure of the difference between the actual output vector and the desired output vector. The error, E_p, for an input–output pattern p is defined as

$$E_p = 1/2 \sum_j (Y_j - d_j)^2, \tag{3}$$

where j is an index over output neurons, Y is the actual state and d is the desired state and $E = \Sigma E_p$ gives the measure of total error. The learning is accomplished in two phases. During the first phase, the input parameters are presented to the input layer and propagated forward so as to compute an output vector. An error estimate for each output unit is obtained by comparing the actual output state with the desired output state. The second phase involves a backward pass through the network during which the error signal is passed to each neuron in the network and appropriate weight changes are made based on generalized delta rule[1].

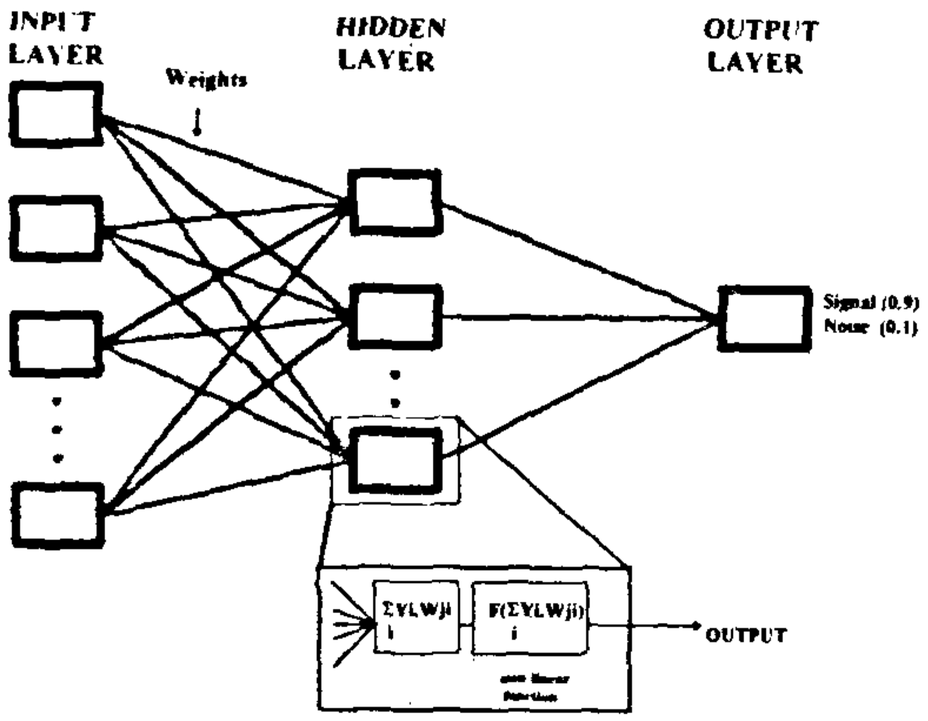

Figure 1. *Architecture of an artificial neural network.*

Training the detection network

Low-order auto regressive (AR) models[5–6] have the ability to represent seismic source functions with a high degree of accuracy[7]. Further, it has been found that the short period seismic noise at GBA can also be represented reasonably well using low-order AR models[8]. Though the model orders are comparable in both these cases, the spectral shapes derived from these models may vary considerably. In order to exploit these spectral differences effectively, spectra derived from 10th order AR models were used as the input to a three-layer ANN for signal detection. The training of the ANN was accomplished with a large set of spectra (0.0–6.0 Hz) derived from the short period data of GBA corresponding to seismic signals from various regions of the globe and seismic noise samples taken at different times of the year. Each training sample was of five seconds duration. The short period digital data from 20 sensors (arranged in the shape of 'L') at GBA have a sampling rate of 20 samples/s per channel. More details on GBA are available elsewhere[9,10].

The ANN has 41 neurons in the input layer, 70 neurons in the hidden layer and 1 neuron in the output layer. Desired output values for noise samples and signals were taken as 0.1 and 0.9 respectively. One could have also chosen these target values as 0 and 1 respectively, however, the system for the given activation function cannot achieve these values without having infinitely large weights[1].

On-line signal detection scheme

The detection process begins with the estimation of AR

spectrum of 5 seconds data corresponding to each working channel of the array. Each spectrum consists of 41 values representing spectral amplitudes at 0.15 Hz interval. From the multi-channel spectra, an average spectrum is computed. Spectral averaging is done mainly to suppress the detection of spurious signals. This spectrum is fed to the input layer of the ANN. A value < 0.5 at the output of the ANN indicates absence of a signal. The detection process continues till a signal is detected (i.e. output of the ANN becomes ≥ 0.5).

Once a signal is detected, the time delays of the signal along the two arms of the array (needed for locating the event)[11,12] are estimated by cross correlating the prediction error filtered data[13,14]. Signal onset times are also estimated using an algorithm based on prediction error filtering and threshold detection techniques[15], which are prerequisites for the post-detection analysis of the seismograms for source identification.

Case studies for signal detection

Figure 2 shows a playout of unprocessed seismic waveforms corresponding to 20 short-period channels of GBA. The waveforms comprise a weak signal around the time indicated by the arrow. The signal emanated from an underground nuclear explosion in Mururoa–Atoll region, South Pacific (mb = 5.1). The signal is not discernible by eye ball search. However, the ANN could distinguish the signal from the background noise. Figure 3 shows the overall beamed sum (using 16 channels) of this event along with the spectrogram of the signal. It may be seen from the figure that signal-to-noise ratio (SNR) in the beamed waveform is close to 2. Considering a value of 0.1 as the average noise correlation at GBA[16], the improvement in SNR turns out as 2.5. This implies that average SNR in a single channel waveform for this event was close to 0.8. The spectrogram, which is a moving window spectral analysis, shows the variations in the spectral contents as one moves the window in steps of 0.5 s. Figure 4 shows the spectra of three preceding noise blocks (5 s each) and the spectrum of the portion comprising the signal (each spectrum is obtained by averaging corresponding multi-channel spectra). It may be seen that the signal and noise spectra practically overlap each other, differing at some frequencies only marginally. Nevertheless, this much deviation was adequate for the ANN to distinguish the weak signal from the background noise.

Figure 5 shows spectra of the preceding noise and the signal portion of another event from the same region (mb = 5.0). Here the signal spectrum has comparatively larger differences with the background noise spectra than the previous event. The signal was duly detected by the ANN.

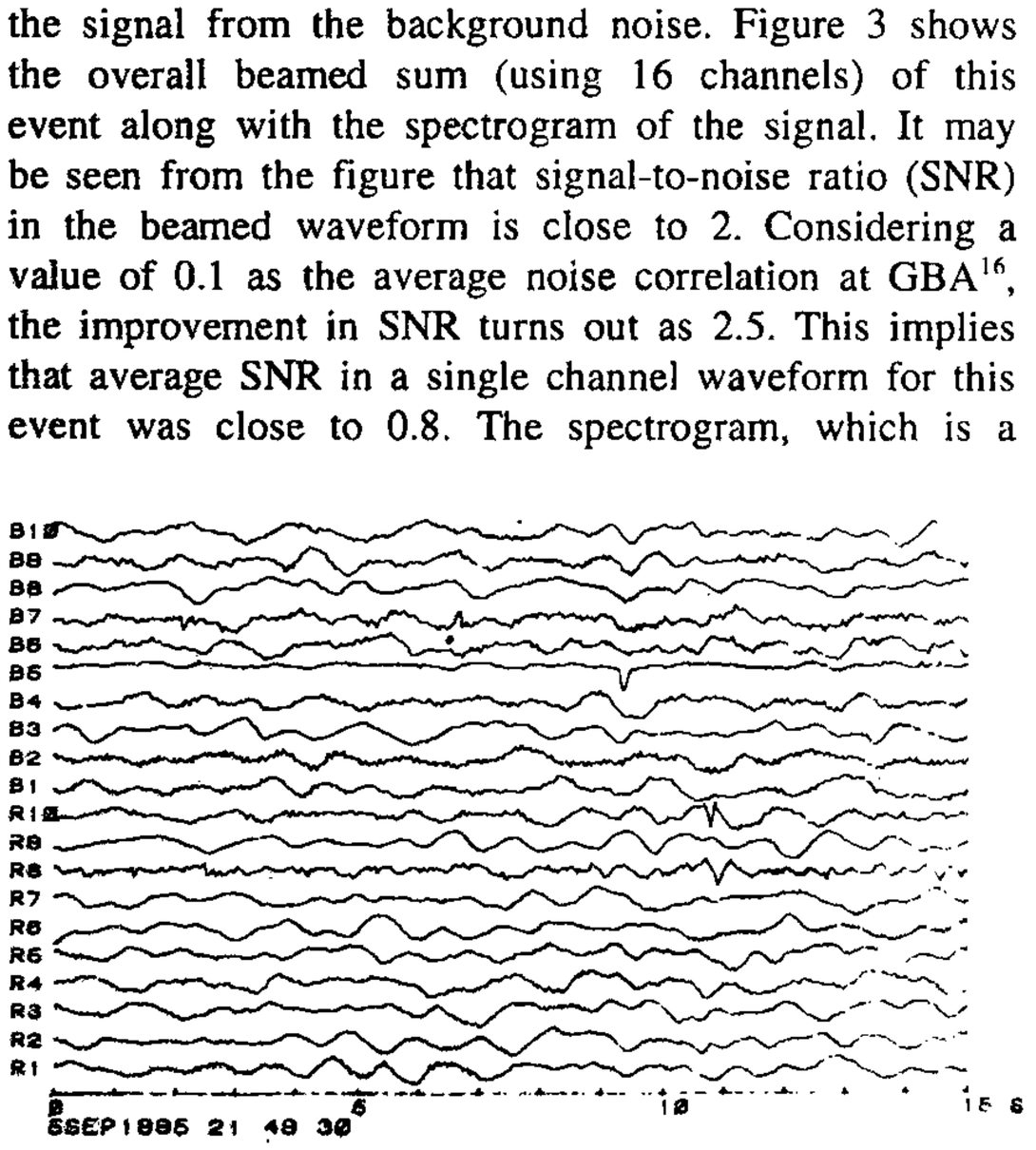

Figure 2. Unprocessed seismograms corresponding to 20 short-period channels of GBA. Arrow indicates expected arrival time of a signal from Mururoa Atolls. Starting time of the waveforms is given at the bottom.

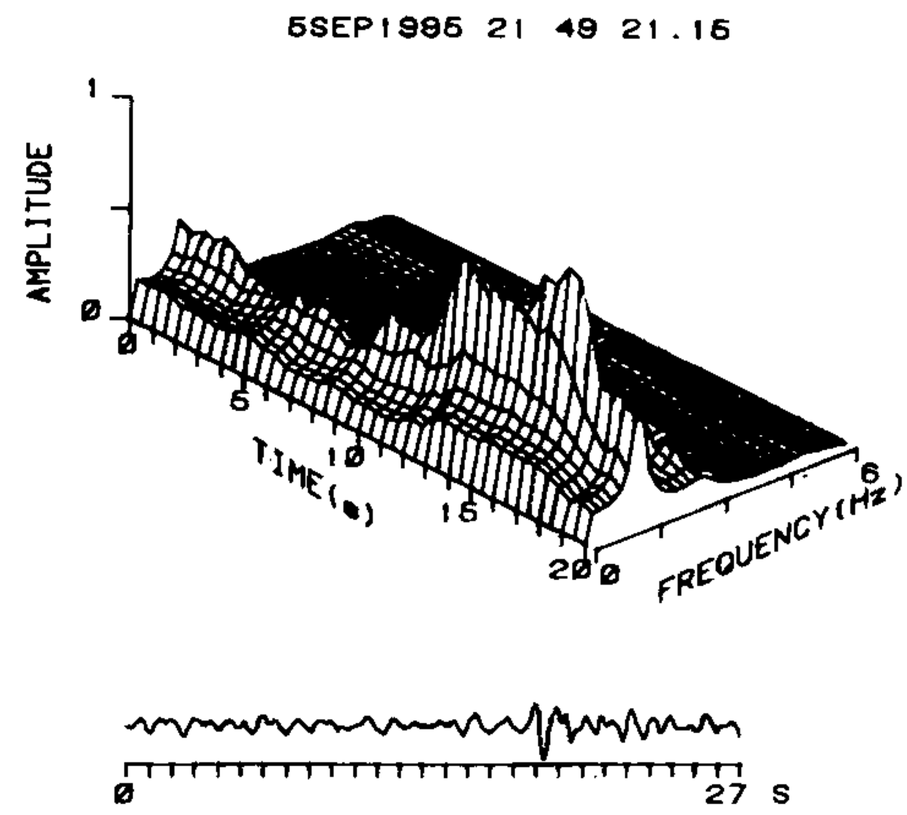

Figure 3. Overall beamed sum of the waveforms shown in Figure 2 along with the corresponding spectrogram. Starting time of the beamed sum is given at the top.

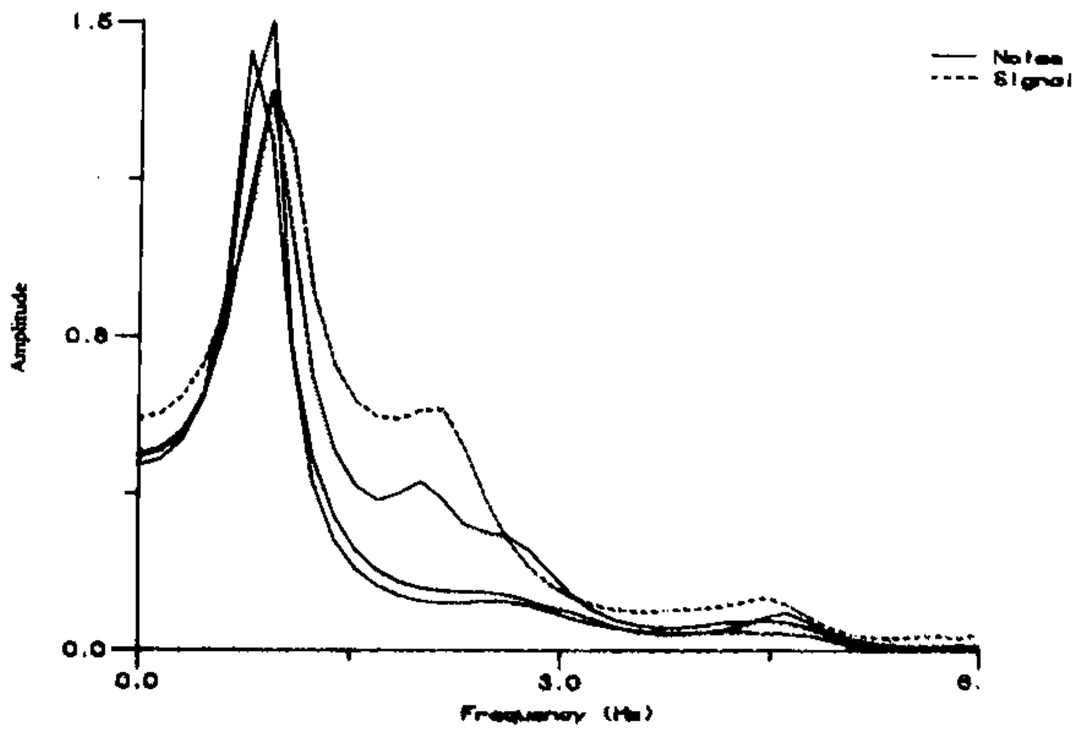

Figure 4. Average AR spectra of noise and signal portions corresponding to the waveforms shown in Figure 2

Spectra corresponding to a larger underground explosion from the same region (mb = 5.2) are shown in Figure 6. Significant differences could be seen between the noise and the signal spectra. This is expected as the event happens to be relatively bigger than the previous ones. The event was detected by the ANN.

Figure 7 shows the waveforms corresponding to a presumed underground explosion (mb = 4.4) in Eastern Kazakh region. Corresponding noise and signal spectra are shown in Figure 8. Signal spectrum could be distinguished from the spectra of the background noise. The event was detected by the ANN.

It may be mentioned here that once an ANN is taught to handle the task of signal detection, its ability to detect a signal does not depend upon the signal strength in the given seismogram. In fact, in a way, the ANN compares the given time series with all the seismograms it had used for learning before it actually converges to a decision. Figure 9 highlights the above point through an illustration. The figure shows the signal spectra corresponding to Figures 4 and 5 along with a noise spectrum of Figure 8. If one looks into the spectra shown in Figures 4 and 5, it will be possible to distinguish the corresponding signal spectrum from the spectra of the preceding noise though with some difficulty. However, when these two signal spectra are compared with the noise spectrum of Figure 8, the task of identifying the signal spectra becomes more difficult. As seen in the figure, the noise spectrum dominates the signal spectra throughout the spectral band, making it difficult for the analyst to differentiate one spectrum from the other. However, it does not pose a problem for the ANN as it has already identified these spectra correctly. Thus in a situation like the one shown in Figure 9, human judgement may fail to identify the spectra correctly but a pre-trained ANN will not. In other words, it may be said that even if the background

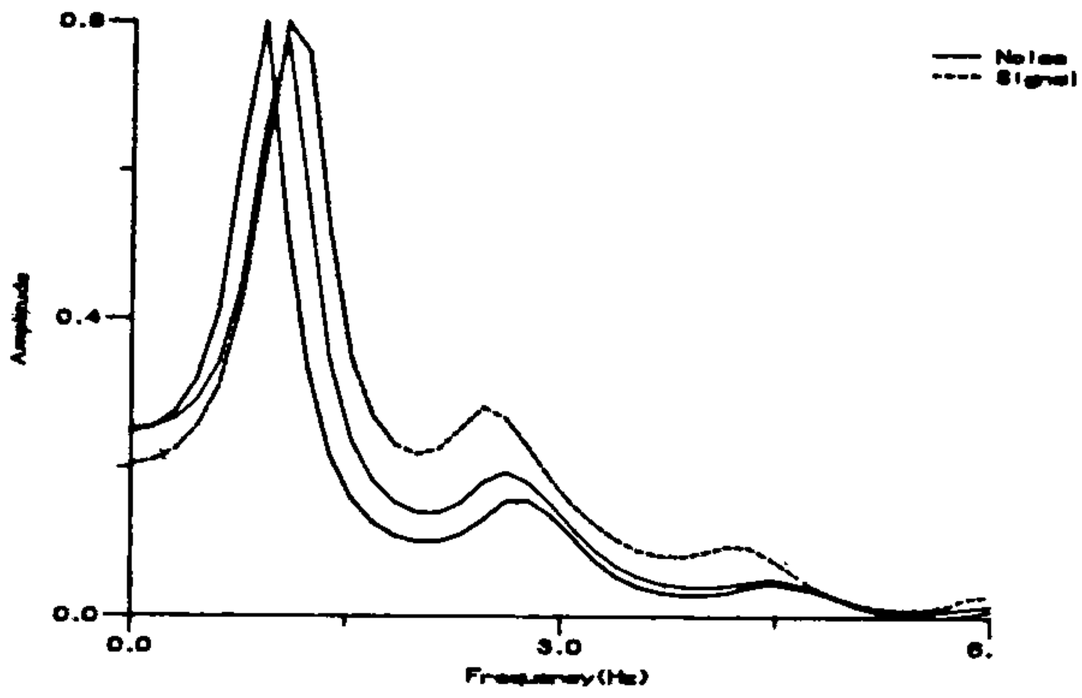

Figure 5. Average AR spectra of noise and signal portions corresponding to another event from Mururoa Atolls.

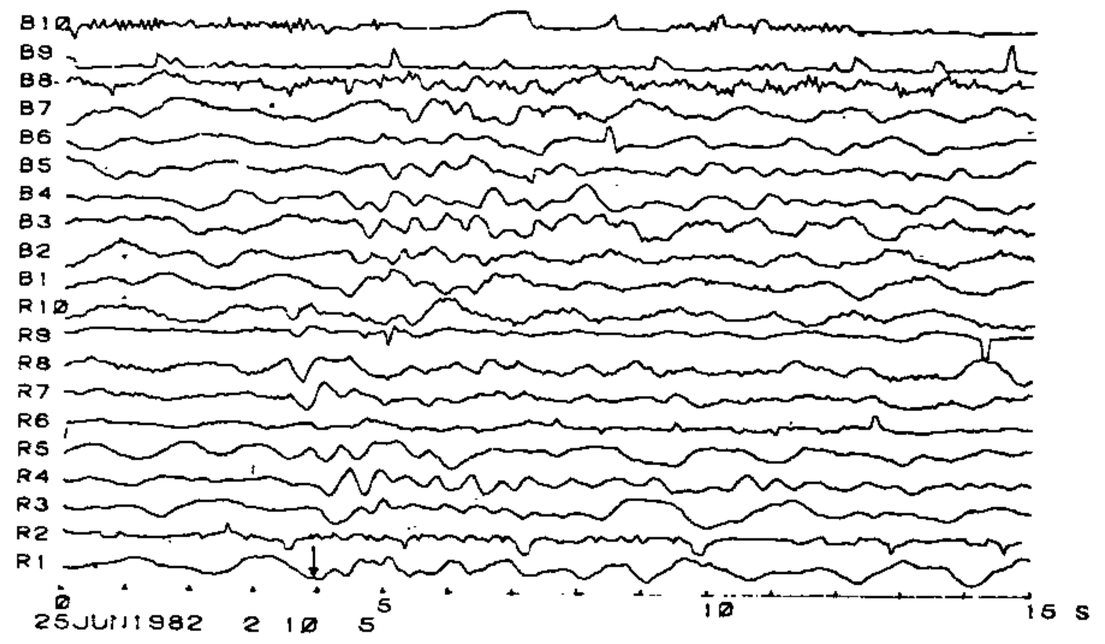

Figure 7. Unprocessed seismograms corresponding to 20 short-period channels of GBA. Arrow indicates expected arrival time of a weak signal from Eastern Kazakh region. Starting time of the waveforms is given at the bottom.

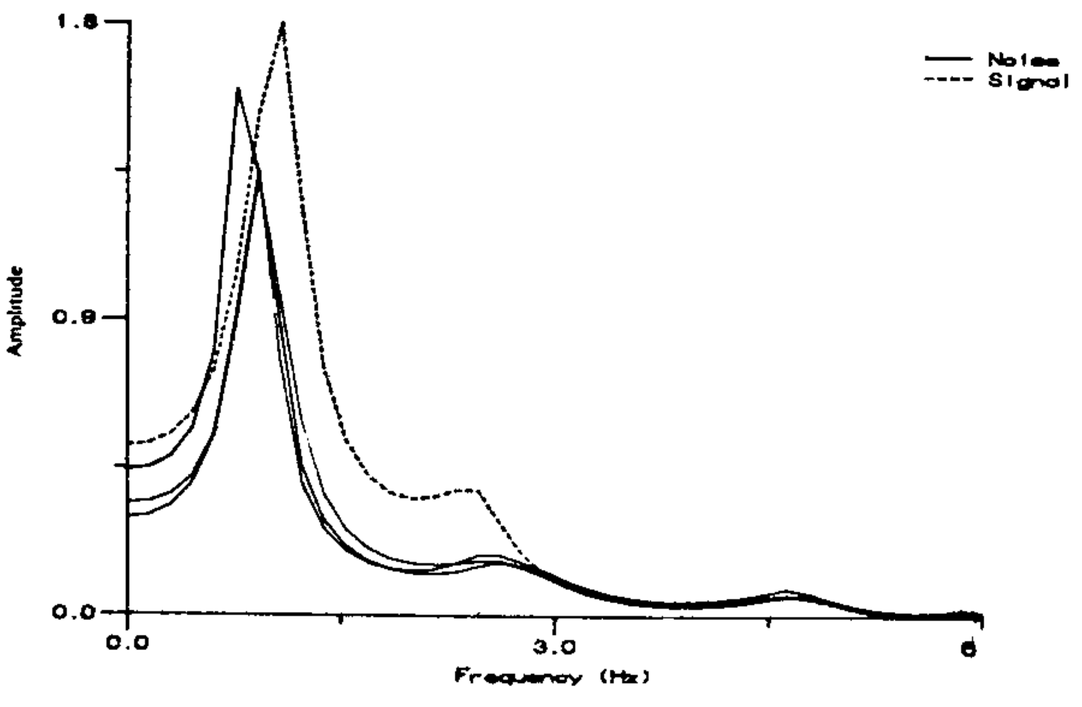

Figure 6. Average AR spectra of noise and signal portions corresponding to a moderate strength event from Mururoa Atolls.

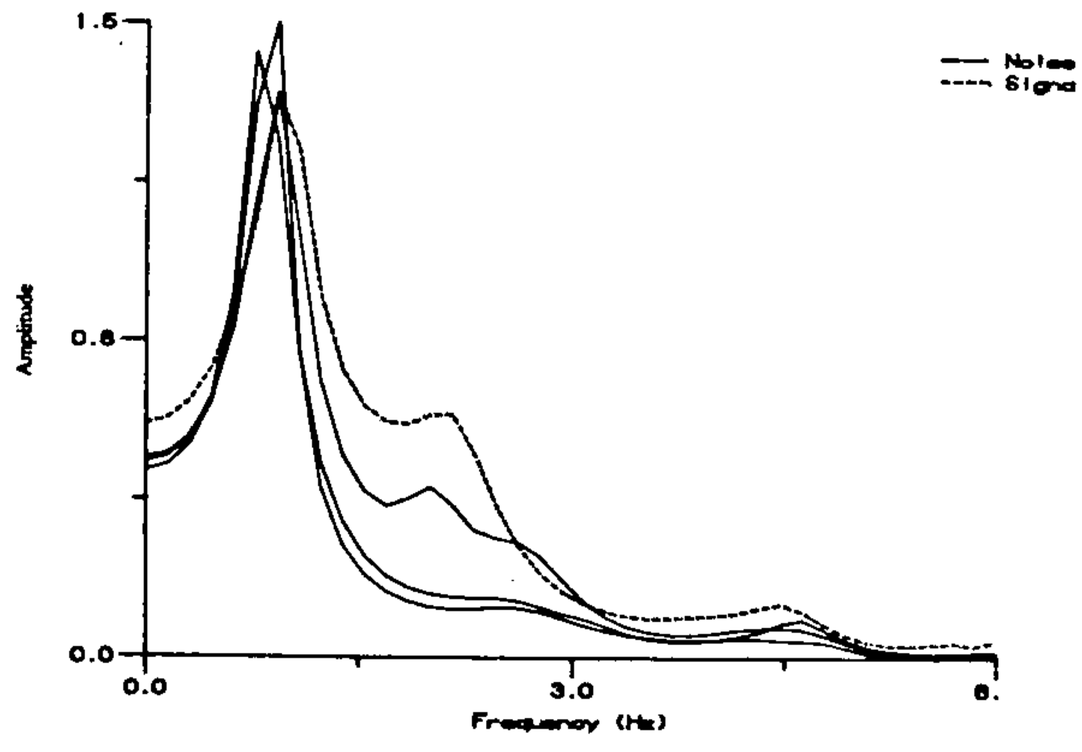

Figure 8. Average AR spectra of noise and signal portions corresponding to the waveforms shown in Figure 7.

noise conditions keep on changing (which is a reality) making the SNR very small, as long as the ANN has been trained with such noise samples, detecting weak signals may not be a problem for the ANN. As already mentioned, an ANN achieves such capabilities through its internal hidden layers.

Advantage of ANN over conventional signal detection methods

In any signal detection process, there is always a trade-off between the number of genuine signals detected and the number of spurious detections. For an on-line system to be effective, the number of spurious detections should be as low as possible. The aim of all the detection processes is to explore the differences between various signal and noise characteristics. In the conventional detection methods which operate on a preset threshold, there are inherent drawbacks. A low value of threshold will detect the weak signals, however, it will result in a large number of spurious detections. On the other hand, a large threshold will fail to detect many weak signals. Detection processes which are based on exploiting the frequency contents of signals and noise have limitations too. Background noise at a recording station is likely to vary with time. Such temporal variations may occasionally get detected as signals.

An ANN detector is more reliable than the conventional ones due to the fact that it is trained using a large set of data comprising various kinds of noise and signals. This takes care of short-term and long-term variations in the noise. The number of spurious detections by an ANN is also negligible. Besides an ANN can be re-trained by including the parameters of the spurious detections, thereby re-adjusting the weights.

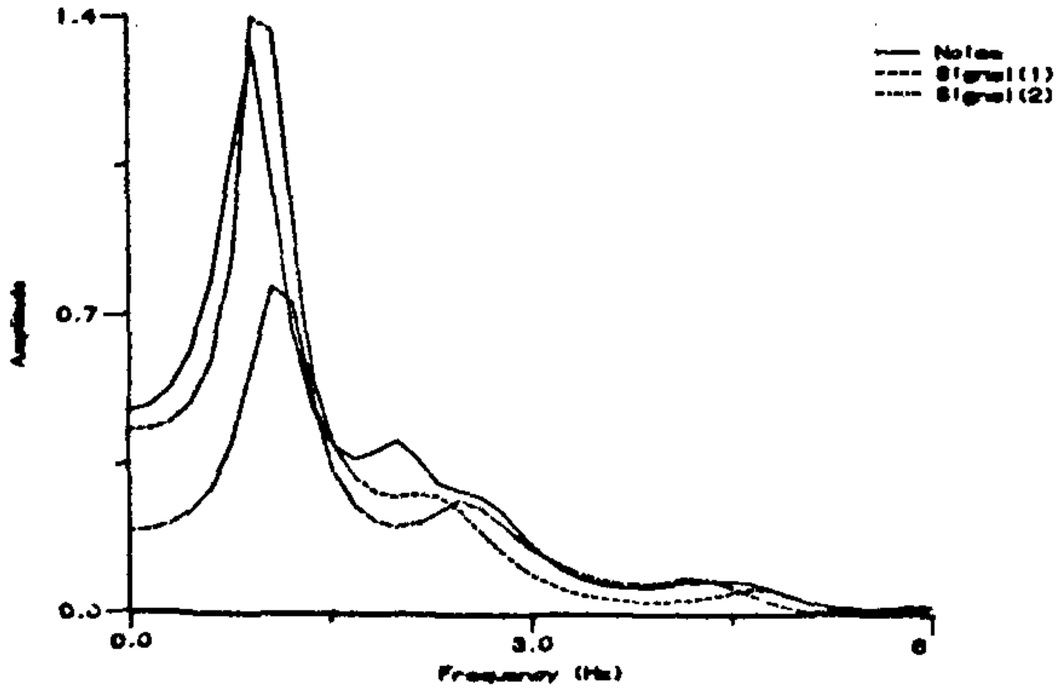

Figure 9. Signal spectra corresponding to Figures 4 and 5 along with a noise spectrum of Figure 8.

Parameters for source identification

As on to-day, for the identification of seismic signals, a large number of SP identifiers are available[17,18], of which some operate in time domain and others in frequency domain. For the present study, some of the established identifiers along with some promising ones based on parametric modelling of seismograms have been used. A brief description of these parameters follow.

Signal complexity

Usually the seismograms generated by underground explosions are much simpler than those generated by the earthquakes of comparable magnitudes. In order to exploit this difference effectively, an identifier known as signal complexity[19], C, is used which is defined as

$$C = \sum_{t=t_2}^{t_3} S(t)^2 / \sum_{t=t_1}^{t_2} S(t)^2,$$

where $S(t)$ denotes the signal amplitude as a function of time. Usually t_1 is taken as the onset of the primary or P-signal. For the present study, the values of t_2 and t_3 have been taken as 3 s and 30 s respectively. Explosion signals are expected to yield a lower value of C compared to the signals from equivalent magnitude earthquakes.

Third moment of frequency

Third moment of frequency[20] (TMF) is a spectral identifier which essentially puts higher weightages on the high frequency components of the seismic signals. It is defined as

$$\mathrm{TMF} = \left[\sum_{f=0}^{5} A(f) f^3 / \sum_{f=0}^{5} A(f) \right]^{1/3},$$

where $A(f)$ is the spectrum of P-signal and f is the frequency in Hz. Explosion signals usually yield larger values of TMF compared to the earthquake signals of comparable strength.

TMF per unit complexity

Explosion signals, in general, have low complexity and high TMF values unlike earthquake signals of equivalent strength. Thus a parameter which is directly proportional to TMF and inversely proportional to complexity will have larger values for the explosions than for the earthquakes of equivalent strength[12,21]. This parameter, CTMF, has been defined as

$$\text{CTMF (C, TMF)} = \text{TMF/C}.$$

TMF, C and CTMF from prediction error-filtered signals

When SNR happens to be low, the contribution of noise to TMF and C cannot be neglected. However, due to their ability to accentuate SNR substantially, prediction error filters (PEFs) can be effectively employed in such situations[13–16]. A prediction error-filtered seismogram, besides having greater SNR, is also richer in high frequencies compared to the unprocessed seismograms. Thus, the identifiers C_p, TMF_p and $CTMF_p$ (suffix 'p' stands for estimates from prediction error filtered seismograms) are expected to aid in the identification of weaker events.

Spectral bandwidth

The differences observed in the seismograms generated by an explosion and an earthquake of comparable strength are primarily due to two important factors, viz. source time function and the source dimension. It is expected that the spectrum of an explosion signal will occupy a larger frequency band compared to the earthquake signal. A typical low-order AR spectrum usually has a smooth shape with a prominent peak. Spectra of earthquake signals are expected to fall off faster beyond the peak value in comparison to the explosion signals. The frequency at which the spectral value falls to 10% of the peak value has been used as one of the identification parameters (SBW).

Shape of prediction error filters

Characteristics of a PEF as computed from *P*-signal of an event are largely controlled by its source function. Due to the basic differences between the explosion and the earthquake source functions, the corresponding PEFs also differ considerably[22]. In order to highlight these differences, a few typical earthquake and explosion signals along with the corresponding PEFs have been shown in Figure 10. It may be seen that the PEFs due to explosions show a 'W' shape at the beginning whereas the PEFs due to earthquakes have a 'V' shape at the beginning. In order to exploit these differences gainfully, angle *BAC* (the angle made by the second, third and fourth sample of the PEF, see Figure 10) has been used as a parameter in combination with the TMF and C of the signals and expressed as

$$\text{P (A, TMF, C)} = (\text{TMF} - k_1)/[A \log \text{C} + k_2 (A + \log \text{C}) + k_3],$$

where A is the magnitude of $\angle A$ and k_1, k_2 and k_3 are constants.

As evident from Figure 10, magnitude of $\angle A$ for explosion PEFs is expected to be lower compared to the earthquake PEFs. The identifier P (A, TMF, C) is expected to yield higher values for an explosion than an earthquake of comparable magnitude. Besides these eight parameters, source distance, azimuth and mb of the events have also been used to train the ANN for signal identification.

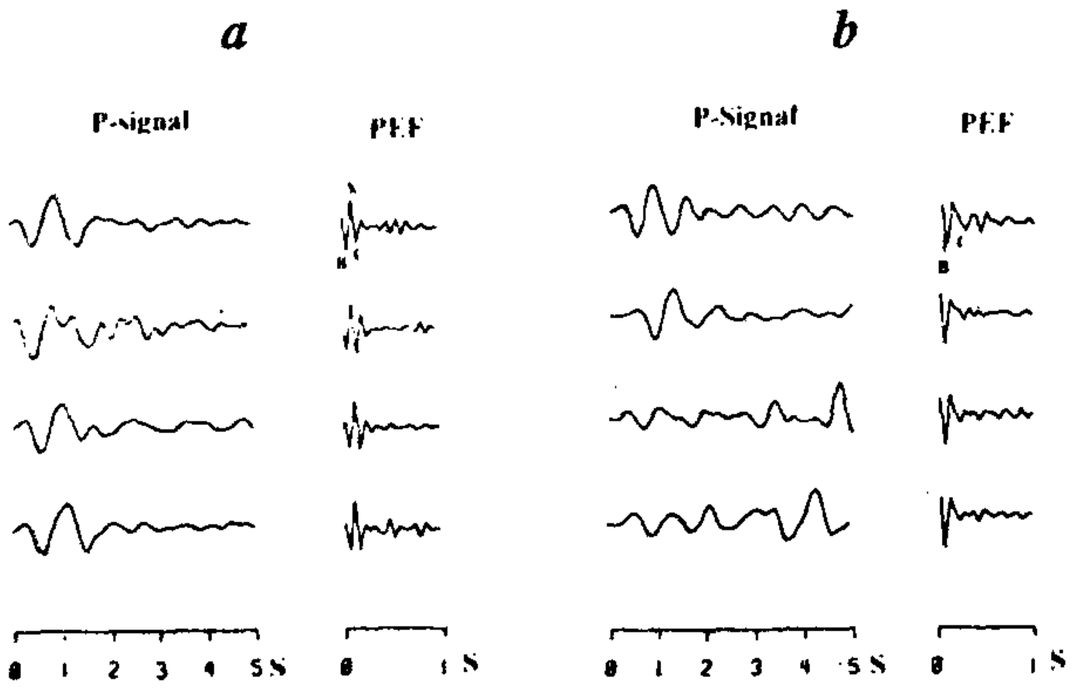

Figure 10. Some explosion signals (*a*) and earthquake signals (*b*) along with the corresponding PEFs.

Training and performance of identification network

Training of the ANN for signal identification has been accomplished with the help of the parameters derived from the SP data pertaining to 206 events. These events comprised both explosions as well as earthquakes and originated at various locations of the globe. The *mb* of these events varied from 3.0 to 6.2. The three-layer identification ANN has 11 input neurons, 150 neurons in the hidden layer and one output neuron. A learning rate of 0.1 was used with 2000 sweeps for training the ANN. The desired output values for earthquake and explosion signals were taken as 0.1 and 0.9 respectively. In order to evaluate the performance of the ANN, another set of sixty events (not used for the training) comprising 30 earthquakes and 30 explosions in the magnitude range 3.5 to 6.2 were analysed using the ANN. All the 60 events were identified correctly by the ANN. Figure 11 shows a few of the signals belonging to this set of data. It may be seen that though the top three earthquake signals appeared explosion-like, the ANN was able to identify them unambiguously. Finally, in order to highlight the capability of these ANNs to detect and identify weak signals in tandem, a seismogram comprising signal

from the Chinese underground explosion (mb = 4.3) of 29 July 1996, has been shown in Figure 12. The event, which originated at a distance of around 30 degrees from GBA, generated very weak signal at GBA. However, the signal was duly detected and identified by the corresponding ANNs.

Performance of the ANN vis-à-vis other identifiers

It has been observed that the most efficient identifiers are applicable to larger events and their efficiency decreases with the event strength. Further, it has been seen that there is no single identifier which is superior to other identifiers in all situations. However, combination of several identifiers usually improves the identification capability.

In order to evaluate the performance of the ANN *vis-à-vis* other identifiers, signals pertaining to 65 Eurasian events comprising 27 earthquakes and 38 explosions were analysed. Number of earthquakes and explosions misclassified by each of the eight identifiers, their combination based on a weighted average (each identifier was assigned a weight based on its performance) and the ANN have been shown in Table 1. It may be seen that even the performance of the combined identifier was no better than some of the individual identifiers for the present data set. However, the ANN could identify all the events successfully.

Conclusions

For training the detection ANN, average signal and noise spectra have been used. Though an average spectrum does not essentially improve SNR, it helps in reducing spurious detections. It may be emphasized that the detection capability of an ANN may be further enhanced by using spectra of array beamed signals. The ANN presented here was able to detect signals from the events having mb as small as 3.0 and originating at a distance of around 2000 km from GBA. The identification ANN has been able to identify events down to mb = 3.5 originating at a distance of around 2000 km from GBA. It is felt that the performance of the identification ANN may be further improved by including

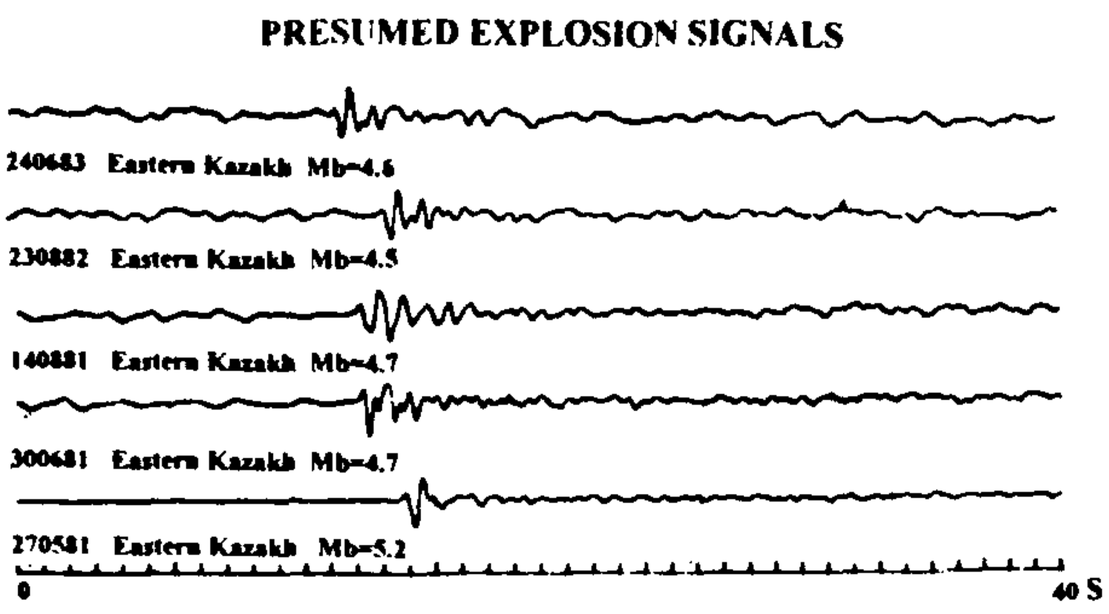

Figure 11. Some earthquake and explosion signals belonging to the set of 60 events which were identified correctly by the ANN.

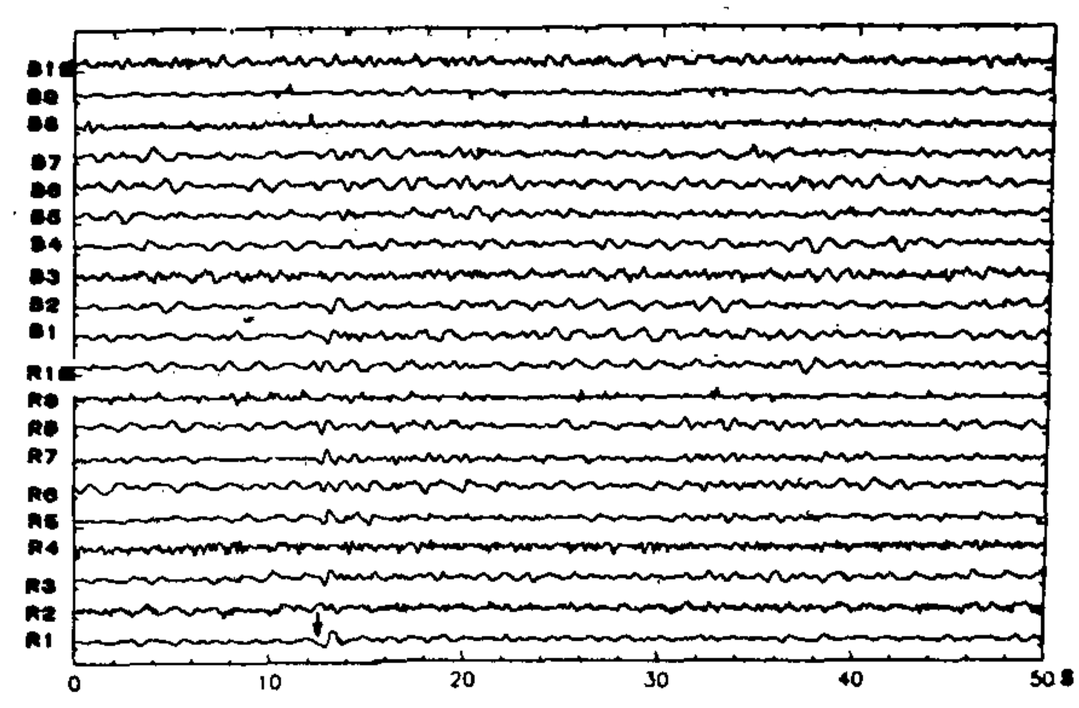

Figure 12. Unprocessed seismogram comprising signal from the Chinese event of 29 July 1996. Arrow indicates the signal onset time.

Table 1. Performance of individual identifiers and their weighted combination *vis-à-vis* the ANN

	Parameters								Weighted comb.	ANN
	C	TMF	CTMF	C_p	TMF_p	$CTMF_p$	SBW	P		
No. of earthquakes misclassified	4	10	4	3	15	2	15	15	4	0
No. of explosions misclassified	2	3	1	2	1	2	1	0	1	0

No. of earthquakes used = 27; No. of explosions used = 38.

parameters derived from the long period and horizontal components of seismic data.

1. Rumelhart, D. E., Hinton, G. E. and Williams, R. J., *Parallel Distributed Processing: Explorations in the Microstructure of Cognition. Vol 1: Foundations* (eds Rumelhart, D. E. and McClelland, J. L.), MIT, Cambridge, 1986, pp. 318–362.
2. Kosko, B., *Neural Networks and Fuzzy Systems – A Dynamical Systems Approach to Machine Intelligence*, Prentice Hall, Englewood Cliffs, NJ, 1992.
3. Zuruda, J. M., *Introduction to Artificial Neural Systems*, West Publishing Co., NY, 1992.
4. Rumelhart, D. E., Hinton, G. E. and Williams, R. J., *Nature*, 1986, **323**, 9.
5. Ulrych, T. J. and Bishop, T. N., *Rev. Geophys. Space Phys.*, 1975, **13**, 183–200.
6. Ulrych, T. J. and Clayton, R. W., *Phys. Earth Planet. Inter.*, 1976, **12**, 188–200.
7. Nair, G. J., *Phys. Earth Planet. Inter.*, 1983, **32**, 36–44.
8. Roy, F., Report No. BARC/1341, 1986.
9. Mowat, W. M. H. and Burch, R. F., Reference No. AWRE/44/47/29, AWRE, Aldermaston, 1974.
10. Varghese, T. G., Roy, F., Rao, B. S. S., Suryavanshi, M. P. and Bharthur, R. N., *Phys. Earth. Planet. Int.*, 1979, **18**, 87–94.
11. Arora, S. K., Report No. BARC/309, 1967.
12. Roy, F. and Basu, T. K., Report No. BARC/E/017, 1994.
13. Murty, G. S., Nair, G. J. and Roy, F., *Mausam*, 1979, **30**, 337–341.
14. Roy, F., *J. Biomed. Eng. Soc. India*, 1990, **12**, 1–10.
15. Roy, F., *Bull. Seismol. Soc. Am.*, 1984, **74**, 1623–1643.
16. Roy, F., Arora, S. K. and Basu, T. K., *Phys. Earth Planet Int.*, 1992, **73**, 264–273.
17. Dahlman, O. and Israelson, H., *Monitoring Underground Nuclear Explosions*, Elsevier, Amsterdam, 1977.
18. Pomeroy, P. W., Best, W. J. and McEvilly, T. V., *Bull. Seismol. Soc. Am.*, 1982, **72**, S89–S129.
19. Kelly, E. J., MIT, Lincoln Lab., Tech. Note 1968-8, 1968.
20. Weichert, D. H., *Z. Geophys.*, 1971, **37**, 147–152.
21. Basu, T. K. and Arora, S. K., Report No. BARC/1348, 1987.
22. Roy, F., Report No. BARC/1475, 1989.

ACKNOWLEDGEMENTS. I am grateful to Dr S. K. Sikka for his encouragement and interest in this work. I thank Dr S. K. Arora for giving some useful suggestions. I also express thanks to Shri R. N. Bharthur, Shri A. G. V. Prasad and Shri E. Unnikrishnan for their help in providing transcripts of digital data of seismograms used in this work.

Received 15 July 1997; revised accepted 31 October 1997

RESEARCH COMMUNICATIONS

X-ray contact microscopic imaging in keV spectral region using laser-produced plasmas

J. A. Chakera†, P. D. Gupta, Yu. Geondgian*, V. V. Sorokin*, V. Yu. Korol* and V. P. Avtonomov*

Centre for Advanced Technology, P.O. CAT, Indore 452 013, India
*P.N. Lebedev Physical Institute, Russian Academy of Sciences, Moscow, Russia

We report here contact microscopic imaging in keV spectral region using pulsed X-ray emission from laser-produced plasmas. The X-ray source was produced by focusing single laser pulses of second harmonic of Nd : glass laser with a peak power of 3 GW in 3 nS (FWHM) on planar targets of copper. Single shot X-ray images of 1 : 1 magnification and an estimated spatial resolution ~ 120 nm were obtained on a ERP-40 photoresist-coated silicon wafer. These images were subsequently viewed under scanning electron microscope and atomic force microscope for high magnification, and with a differential interference contrast optical microscope for colour contrast. Details of the imaging technique are presented, and images recorded for yeast cells are given as an example.

X-RAY contact microscopy has recently drawn considerable attention for imaging biological cells with high spatial resolution[1–3]. This is because in conventional optical microscopy, the spatial resolution is limited by the wavelength of illuminating radiation to ~ 0.5 μm. In electron microscopy, it is not possible to image biological cells in their natural living conditions due to the necessity of slicing, dehydration, and staining of the sample to obtain a good contrast. In comparison, X-ray contact imaging in the so-called water window spectral region (from 2.3 nm to 4.4 nm corresponding to K-absorption edges of oxygen and carbon respectively) can provide high contrast images in presence of water. Many authors[1–7] have reported on X-ray contact microscopic imaging of biological samples using X-rays in this spectral region.

An important potential application of X-ray microscopic imaging can be in elemental mapping of a sample[1,3]. The idea is based on difference imaging of the sample using X-rays in two different spectral regions on either side of an absorption edge of an element in the sample under investigation. However, since K and L absorption edges of many elements of interest occur at $\lambda < 1$ nm, one has to use an X-ray source in keV spectral region. Moreover, a large variety of biological cells have a size of several microns, in which case X-rays in the water-window spectral region would be strongly attenuated[3]. Thus, X-ray microscopic imaging using radiation of $\lambda < 1$ nm can be of considerable practical interest. However, much less attention has been paid to X-ray contact microscopic imaging in this spectral range.

†For correspondence.